Astron. Nachr. / AN **333**, No. 9, 796 – 809 (2012) / **DOI** 10.1002/asna.201211725

The 1.5 meter solar telescope GREGOR

W. Schmidt[1,⋆], **O. von der Lühe**[1], **R. Volkmer**[1], **C. Denker**[3], **S.K. Solanki**[4], **H. Balthasar**[3], **N. Bello Gonzalez**[1], **Th. Berkefeld**[1], **M. Collados**[5], **A. Fischer**[1], **C. Halbgewachs**[1], **F. Heidecke**[1], **A. Hofmann**[3], **F. Kneer**[2], **A. Lagg**[4], **H. Nicklas**[2], **E. Popow**[3], **K.G. Puschmann**[3], **D. Schmidt**[1], **M. Sigwarth**[1], **M. Sobotka**[6], **D. Soltau**[1], **J. Staude**[3], **K.G. Strassmeier**[3], and **T.A. Waldmann**[1]

[1] Kiepenheuer-Institut für Sonnenphysik, Schöneckstraße 6, 79104 Freiburg, Germany
[2] Institut für Astrophysik der Georg-August-Universität Göttingen, Friedrich-Hund-Platz 1, 37077 Göttingen, Germany
[3] Leibniz-Institut für Astrophysik, An der Sternwarte 16, 14482 Potsdam, Germany
[4] Max-Planck-Institut für Sonnensystemforschung, Max-Planck-Straße 2, 37191 Katlenburg-Lindau, Germany
[5] Instituto de Astrofísica de Canarias, Vía Láctea, 38200 La Laguna (Tenerife), Spain
[6] Astronomical Institute AS CR, Fričova 298, 25165 Ondřejov, Czech Republic

Received 2012 Aug 30, accepted 2012 Sep 23
Published online 2012 Nov 2

Key words instrumentation: high angular resolution – Sun: magnetic fields – telescopes

The 1.5 m telescope GREGOR opens a new window to the understanding of solar small-scale magnetism. The first light instrumentation includes the Gregor Fabry Pérot Interferometer (GFPI), a filter spectro-polarimeter for the visible wavelength range, the GRating Infrared Spectro-polarimeter (GRIS) and the Broad-Band Imager (BBI). The excellent performance of the first two instruments has already been demonstrated at the Vacuum Tower Telescope. GREGOR is Europe's largest solar telescope and number 3 in the world. Its all-reflective Gregory design provides a large wavelength coverage from the near UV up to at least 5 microns. The field of view has a diameter of 150″. GREGOR is equipped with a high-order adaptive optics system, with a subaperture size of 10 cm, and a deformable mirror with 256 actuators. The science goals are focused on, but not limited to, solar magnetism. GREGOR allows us to measure the emergence and disappearance of magnetic flux at the solar surface at spatial scales well below 100 km. Thanks to its spectro-polarimetric capabilities, GREGOR will measure the interaction between the plasma flows, different kinds of waves, and the magnetic field. This will foster our understanding of the processes that heat the chromosphere and the outer layers of the solar atmosphere. Observations of the surface magnetic field at very small spatial scales will shed light on the variability of the solar brightness.

1 Introduction

The installation of the 1.5 m solar telescope GREGOR at the Observatorio del Teide (OT) is a major milestone for solar physics in Europe. Not only is GREGOR Europe's largest and most powerful solar telescope, it also forms, together with the neighboring 70 cm Vacuum Tower Telescope (VTT) and the 90 cm THEMIS, the world's most powerful set of solar telescopes at a single site. Figure 1 shows an aerial view of the OT with the three large solar telescopes aligned along the ridge, with THEMIS in the lower right corner of the image, followed by the VTT and GREGOR.

First ideas to build a telescope of the 1.5 meter class, to replace the 45 cm Gregory-Coudé telescope were presented in 1997. The abstract of a GREGOR flyer, prepared in late 1999 reads:

GREGOR is a large solar telescope with an aperture of 1.5 m. It is equipped with adaptive optics and a polarimetry system. It is designed for high-precision measurements of the magnetic field and the gas motion in the solar photosphere and chromosphere with a resolution of 70 km on the Sun, equivalent to the photon mean-free path in the photosphere. GREGOR will be installed at the Observatorio del Teide, Tenerife. The focal plane instrumentation includes a high resolution filter spectrometer and a polarimetric spectrograph for the visible and the near-UV spectral range.

The official proposal was prepared in March 2000. From the beginning, it was clear that the new telescope would not continue the route of evacuated telescopes, but would be an open one (von der Lühe et al. 2000). This change of paradigm had important consequences, and led to the decision to have a removable dome to allow for air flushing. Mirror seeing on the primary was a major concern, therefore a mirror from a novel material, silicon carbide, was envisioned, in order to facilitate cooling from the backside. The open dome concept was realized, but unfortunately, the silicon carbide solution failed, for technical reasons. The finally installed primary mirror is now made of lightweighted Zerodur, also with backside cooling. A retrospective of the GREGOR project and an overview of the corresponding literature can be found in Kneer (2012) and in Denker et al. (2012).

⋆ Corresponding author: wolfgang@kis.uni-freiburg.de

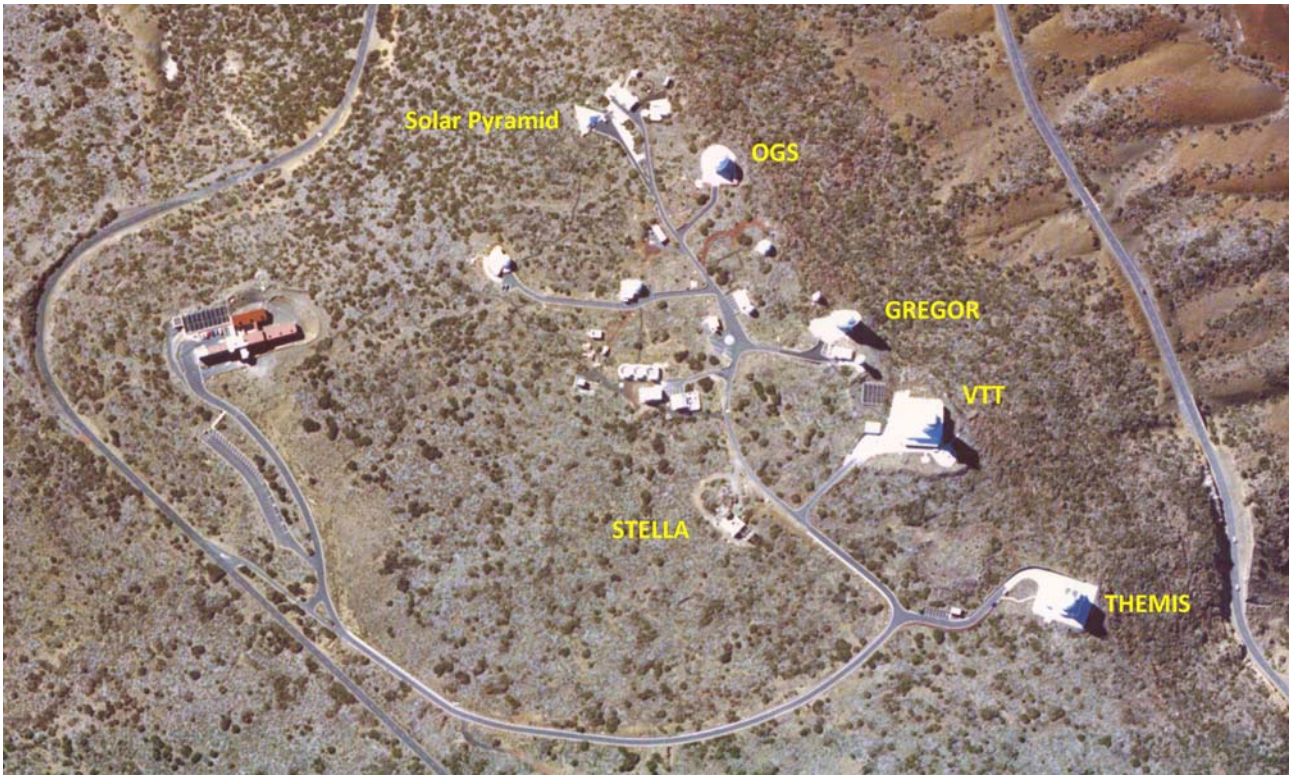

Fig. 1 (online colour at: www.an-journal.org) Aerial view of the Observatorio del Teide in Izaña, Tenerife, with the solar telescopes (from bottom right diagonally along the ridge) THEMIS, VTT, and GREGOR. The fourth large building at some distance of GREOR is the Optical Ground Station (OGS) of ESA. Small synoptic solar telescopes are installed adjacent to the OGS. The STELLA installation is located just opposite of the access road to the VTT. The Residencia of the IAC is seen in the left part of the image.

After about 10 years of planning, construction, and installation, the final pieces of GREGOR and its first-light instruments were installed in 2011, and the science verification started in spring of 2012. Delays with the telescope optics allowed installing and test parts of the focal-plane instruments, as well as the adaptive optics already in 2010. For these tests, a 1-meter mirror[1] with the same focal length as the original primary mirror, was installed. As a result, the telescope was ready for science verification only a few months after the installation of the primary mirror.

In the following sections, we present an overview of the GREGOR solar telescope and its focal-plane instruments. Section 2 summarizes the science goals of GREGOR. In Sect. 3 the most important aspects of building, dome and telescope structure are briefly described, and references for further reading are given. The first-light instruments and their capabilities are described in Sect. 4. The final section provides an outlook to second-generation instruments.

2 Science with GREGOR

Magnetic fields control many processes on the Sun and its variability. Knowledge about the generation of the solar magnetic field, its dynamical behavior and its disappearance from the solar surface is therefore indispensable for our understanding of the Sun. In the photosphere, magnetic fields are visible at a variety of spatial scales and a range of life times. The most prominent objects, the sunspots, have been observed ever since the invention of the telescope, and these observations led to the discovery of the solar cycle, well before the magnetic origin of that cycle became known. In 1908, sunspots were the first extraterrestrial objects where strong magnetic field could be measured. Nowadays, measurements of the cyclical behavior of the number, polarity, and location of sunspots provide an important test bed for solar and stellar dynamos. To date, no convincing or conclusive theory for the solar activity cycle exists. Besides the 22-year magnetic cycle, longer cycles of solar activity may exist, but none of these long-term changes can be predicted with any certainty. The situation is not much different toward shorter time scales. The life cycle of sunspots spans a range from several hours up to three months, whereas the formation process itself takes only a few hours. Thanks to space-borne observatories and the much improved spatial resolution of ground-based facilities, high-quality observational data do now exist, but still not enough to allow for a convincing theoretical or numerical model of sunspot formation.

[1] This 1 m mirror, made of CESIC, was a prototype mirror for space applications, and was made available to the GREGOR project by the Lockheed Martin Solar and Astrophysics Lab (Palo Alto, USA).

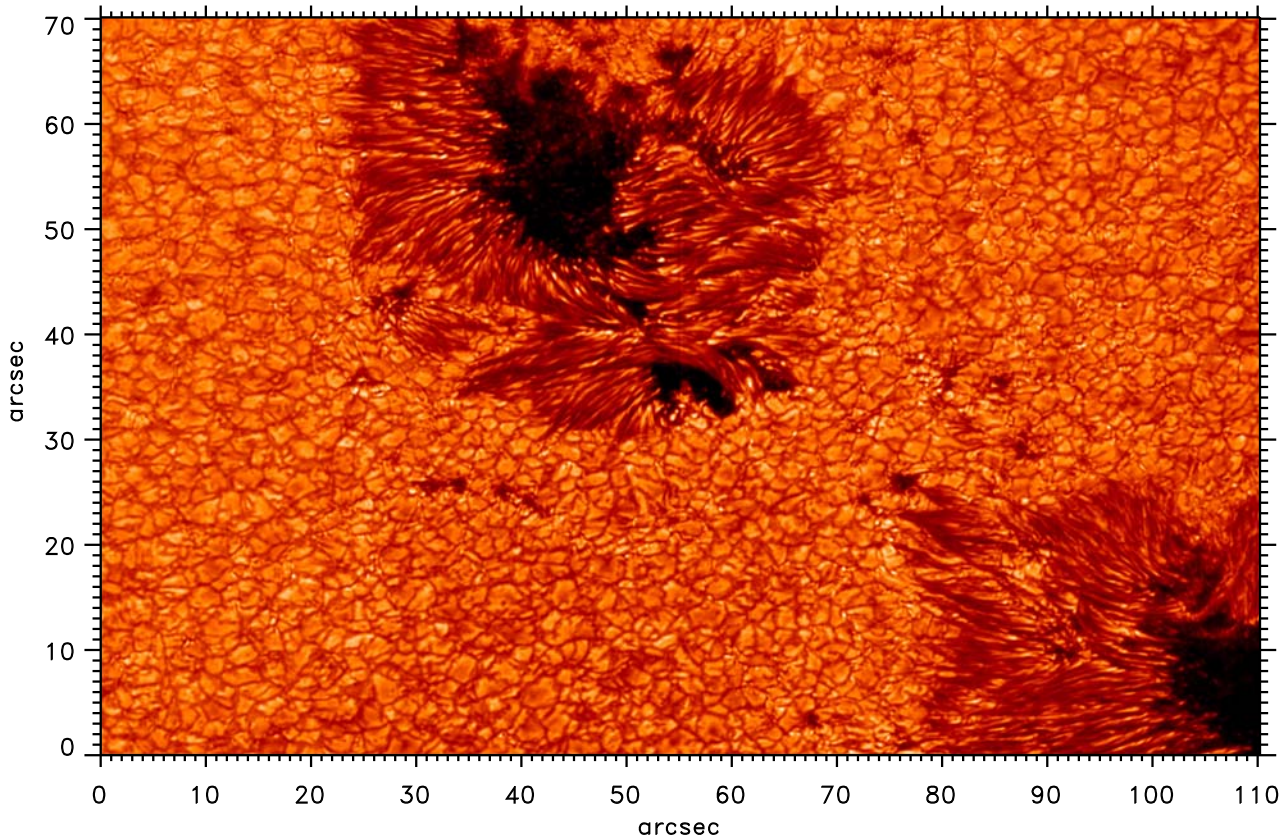

Fig. 2 (online colour at: www.an-journal.org) Sunspot (AR 111504, $\mu = 0.72$) observed with the GREGOR Broad-Band Imager on 17 June 2012 at a wavelength of 590 nm.

The good coverage of observation from space, especially from SOHO (Scherrer et al. 1995), and recently from SDO (Scherrer et al. 2012) provided a wealth of data on solar magnetism on spatial scales larger than, say, one arcsecond. These scales are important to understand the general behavior of the magnetic field, provide information about the motion of the magnetic field relative to the plasma, and give insight into the dynamics of active regions as a whole. A large fraction of the magnetic flux on the Sun is located at spatial scales below one arc second, and at these scales, time scales below one minute become relevant. Observations of the Sun's magnetic field at high spatial and temporal resolution are therefore of highest importance for a full understanding of solar magnetism.

For the past few years, data from the Solar Optical Telescope of the Japanese HINODE satellite (Kosugi et al. 2007), from the Swedish Solar Telescope (Scharmer et al. 2003), and from the balloon-borne Sunrise telescope (Barthol et al. 2011; Schmidt et al. 2010b; Solanki et al. 2010) delivered new insights into the small-scale magnetism of the solar photosphere and lower chromosphere. Nevertheless, the science objectives, formulated in the original GREGOR proposal in the year 2000, are still valid. Since then, the importance of high-quality spectropolarimetric observations has even grown.

For precise measurements of the magnetic field in the chromosphere, an aperture of one meter is not sufficient, since the outer atmosphere is probed with very strong spectral lines with line-core intensities of a tenth or less of the photospheric intensity. For a high photometric accuracy, sufficient photon flux is needed. Compared to the 70 cm VTT, GREGOR will provide a substantial increase in photon flux and hence enable high-quality measurements of the magnetic field in the chromosphere. The increase of photon flux with increasing aperture holds for a certain area on the Sun (Schmidt et al. 2012). An area of 100×100 km^2 on the Sun observed with GREGOR delivers four times more photons to the focal plane than the VTT.

Large-aperture telescopes like GREOR are needed for at least two reasons: (1) to provide sufficient photon flux for a given area on the Sun to allow for high-precision measurements of the magnetic field, and (2) to push the spatial resolution down to a few tens of kilometers to spatially resolve small magnetic flux concentrations. The instrumentation of GREGOR allows to choose from these options, or to use a compromise between the two extremes.

2.1 Science objectives

In a nutshell, the science objectives of GREGOR are the following ones:

To study the interaction between convection and the magnetic field in the photosphere. In the quiet photosphere, the most important themes are the emergence and removal of magnetic flux and the interaction of the small-scale magnetic flux concentrations with the convective motion – the granulation – at the surface. Kilogauss magnetic flux concentrations are observed in granular lanes. According to numerical simulations, their spatial scales are of the order of 100 km, or below (Grossmann-Doerth et al. 1998; Hasan et al. 2005). Lagg et al. (2010) investigated the properties of magnetic flux tubes observed with the IMaX instrument onboard the balloon-borne Sunrise telescope. They confirm a field strength of 1.45 kG and a size of 0.15″. However, follow-up work on Sunrise data by Riethmüller et al. (2010) has shown that many smaller magnetic features associated with bright points exist that have most likely not been resolved. This underlines the need for a larger telescope. The true nature of internetwork fields and their origin (are they produced by a global or a local dynamo) is another important open question (see de Wijn et al. 2009, for a review). Using data from the Sunrise balloon observatory, Steiner et al. (2010) have observed horizontal vortices, causing bright lanes across granules. For a proper understanding of this phenomenon, sequences with highest spatial resolution are needed.

To understand the fine structure of sunspots. This topic includes the structure and dynamics of sunspots with their complex flow and magnetic field patterns. In the umbra, umbral dots are embedded in the cool and strongly magnetized plasma, and light bridges exhibit their own dynamical pattern. Although the observations of Riethmüller et al. (2008) and Bharti et al. (2009) suggest that umbral dots are magnetoconvective structures, as proposed by Schüssler & Vögler (2006), the downflows predicted by the simulations are critical and have remained elusive until now. Sunspot penumbrae show the well-known radially oriented Evershed flow, and magnetic fields of different inclinations, horizontally and vertically interlaced. Dark lanes, embedded in bright penumbral filaments have been found in high-resolution images (Scharmer et al. 2002). Spectro-polarimetric observations with highest resolution are needed to understand the physical nature of these lanes, as well as to test models such as that of Spruit & Scharmer (2006) and to determine the nature of the cool downflows found by Franz & Schlichenmaier (2009), Joshi et al. (2011) and Scharmer et al. (2011). Finally, the formation of sunspot penumbrae, whose complexity has been demonstrated by the excellent data gathered at the VTT (Rezaei et al. 2012b), remains an important open question awaiting its resolution with the help of higher resolution data.

To uncover the role played by the solar magnetism in causing solar variability. At the maximum of an 11-year activity cycle, the solar constant is higher by about 0.1 % compared to its value at activity minimum (see e.g. Fröhlich 2006; Krivova et al. 2006). This number holds for spatially and spectrally integrated light. In the UV, the variation is much stronger. The increase of the total brightness at activity maximum is caused by small-scale faculae with angular sizes on the order of 0.1″, whose effect more than compensates the influence of cool sunspots. It has been shown in the last decade that total solar irradiance variations are caused by magnetic fields at the solar surface (Ball et al. 2012; Krivova et al. 2003; Wenzler et al. 2006). Nonetheless, the data from the most recent set of spectral solar irradiance instruments (SIM and SOLSTICE on SORCE, Harder et al. 2005; Woods & Rottman 2005) are rather at variance with all models on the solar cycle time scale (Ball et al. 2011). Only simultaneous high-resolution measurements of the brightness and magnetic properties of small-scale magnetic features as well as of their surroundings at multiple wavelengths will enable this discrepancy to be resolved. A long-term decline of solar activity, similar to the Maunder minimum, has been predicted (Penn & Livingston 2011), but a very recent work by Rezaei et al. (2012a) shows that the decline observed during cycle 23 is most probably part of a cyclic variation. Accurate measurements of sunspot magnetic fields during the present activity cycle are needed to clarify this issue.

To understand the enigmatic heating mechanisms of the chromosphere. There has been substantial progress in the observation of chromospheric structure and dynamics (Judge et al. 2010; Rutten 2010; Wedemeyer-Böhm et al. 2009), and some measurements of the chromospheric magnetic field have been made (Harvey 2009). Nevertheless, the relative importance of the magnetic field and acoustic waves for the heating of the chromosphere is still under intense discussion (Bello González et al. 2010; Carlsson 2007). Swirling motions were recently found in the photosphere and also in the chromosphere. They may be another mechanism to transport energy from the solar surface to higher layers of the solar atmosphere (Wedemeyer-Böhm et al. 2012). The time scales of chromospheric dynamics are short, the magnetic field is small, and the light level is low: these are the ingredients of an observational challenge that can only be met by a large-aperture solar telescope.

To search for solar twins. Stellar statistics indicate the existence of about one billion G2 stars in our galaxy, or 3000 such stars within a radius of 250 light years around the Sun. To date, only few solar twins have been spectroscopically identified. Night-time observations with GREGOR will be used for a large spectroscopic survey to study e.g. the evolution of the angular momentum of solar twins. Target regions will be open clusters that were characterized in the STELLA Open Cluster Survey (Fügner et al. 2011).

3 Telescope

The proven concept of solar telescopes with evacuated tubes to avoid mirror seeing is not applicable to telescopes with apertures significantly above one meter. The pressure difference at the large entrance window would cause stress-induced birefringence which would severely impact polari-

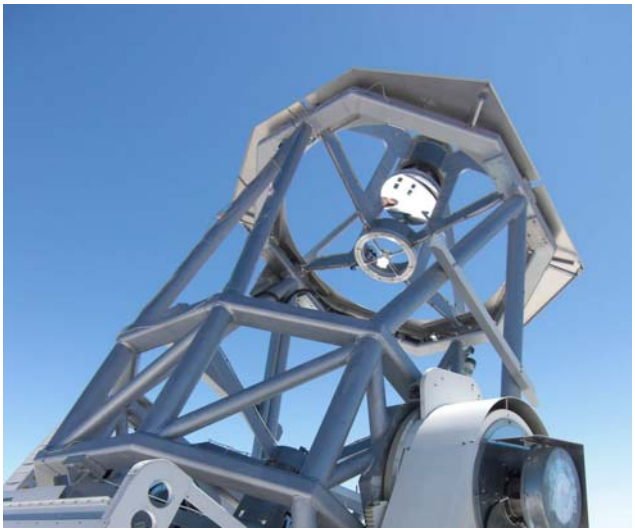

Fig. 3 (online colour at: www.an-journal.org) The GREGOR telescope pointed to the Sun. M2 is seen in the top right part of the picture. Below M2, there is the primary field stop that reflects most of the light out of the telescope.

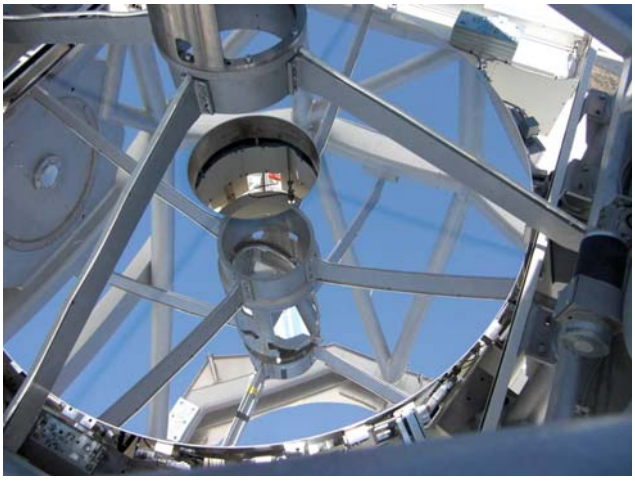

Fig. 4 (online colour at: www.an-journal.org) Primary mirror and some of the spiders.

metric measurements. This is one of the reasons, why the two newest solar telescopes with apertures above one meter, GREGOR at the Observatorio del Teide, and the 1.6-meter NST (Cao et al. 2010) at Big Bear Observatory in the US, were built as open telescopes. The NST and GREGOR use different approaches to prevent dome seeing. While GREGOR has a retractable dome and uses wind flushing of the telescope area to remove near-telescope turbulence, the NST has a closed dome with active venting. The NST optical off-axis design is quite similar to that of the Advanced Technology Solar Telescope (ATST, Keil et al. 2010), whereas GREGOR with its on-axis optics can be considered a pathfinder design for the European Solar Telescope (EST, Collados et al. 2010).

3.1 Optical design

GREGOR is a double Gregory system with three imaging mirrors (Soltau et al. 2012). The optical design is similar to that of the LEST telescope concept (Engvold & Andersen 1990). The primary mirror has a diameter of 150 cm and a focal length of 2.5 m. In the primary focal plane, an image of the solar disk with a diameter of 25 mm is formed, with a total power of about 2000 W, and a flux density of about 6 MW/m^2. At this location, a water-cooled field stop (Fig. 3) deflects most of the sunlight out of the telescope, and transmits a circular field-of-view with a diameter of 150″ through a central hole. In order to decrease the heat load on the field stop, the reflecting surface will be coated with protected silver, to enhance the reflectivity and thereby reduce the absorption. The elliptical secondary mirror forms a secondary image near the intersection of the optical and the elevation axis of the telescope. At this place, the (removable) GREGOR Polarization calibration Unit (GPU, Hofmann et al. 2012) is located. The beam continues to the second elliptical mirror M3, which forms the final image at the focus, F3. The folding flat M4 directs the light beam into the elevation axis, and additional flat folding mirrors direct the beam further to the observing laboratory one floor below the telescope platform (Volkmer et al. 2006; von der Lühe et al. 2000). Figure 4 shows the primary mirror M1. The reflected image from M1 shows some of the spiders, and the inclined plane mirror M4 (Fig. 5). Since the alt-azimuth mount delivers a rotating solar image at F3, it is foreseen to install an optional image de-rotator between the exit window of the telescope and F3.

3.2 Telescope structure

The telescope structure is a very stiff steel construction which keeps the optical components of the telescope well aligned, independent of the orientation of the telescope. The structure, and the alt-azimuthal mount are stiff enough to allow for precise pointing at wind speeds up to 15 m/s. All sun-lit parts are painted in white, to minimize deformation caused by heating effects. The secondary mirror M2 is mounted on a hexapod which can be moved in six degrees of freedom, in order to maintain good alignment between the primary and secondary mirror (see Volkmer et al. 2012, for details). The alignment of M2 is controlled in closed loop using the wavefront sensor of the AO.

3.3 Telescope control system

The GREGOR Telescope Control System is setup in a modular way (Halbgewachs et al. 2012). Pointing to the Sun is automatic, based on ephemeris computation and an experimentally derived pointing model (Granzer et al. 2012), i.e. without the use of a guider telescope. For accurate tracking of features on the solar disk, either (cartesian) disk coordinates or heliographic coordinates can be specified. For nighttime observations, object coordinates should be given in right ascension and declination. Object coordinates can

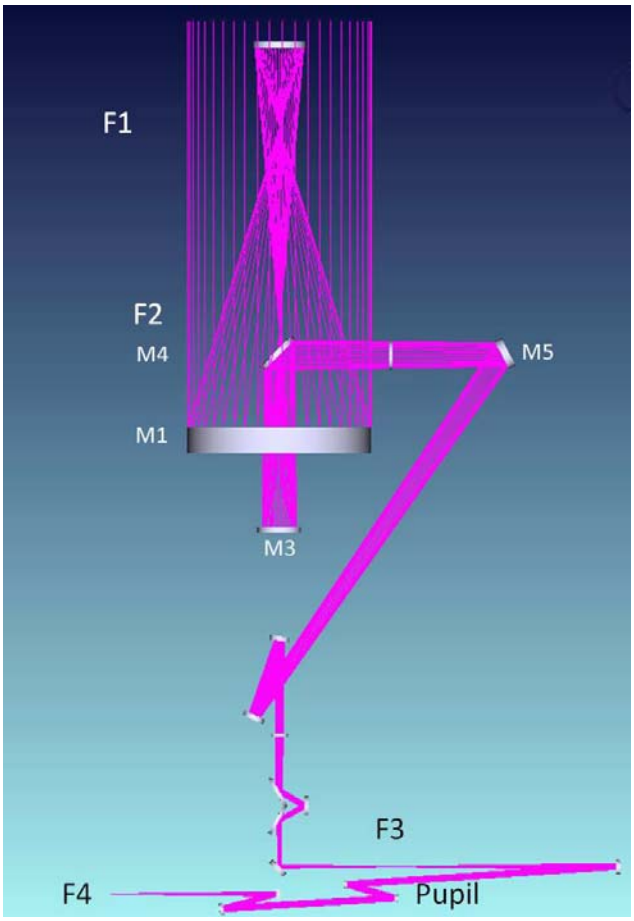

Fig. 5 (online colour at: www.an-journal.org) Optical design of GREGOR. F1 to F3 denote the focal planes of the telescope, The adaptive optics reimages F3 to F4.

also be saved in tracking lists (and restored from there), to simplify observation procedures.

3.4 Building and enclosure

In order not to open a Pandora's box concerning construction permits, environmental impact studies and the like, we decided early in the project, to install the new telescope on top of the existing building of the 45 cm Gregory-Coudé telescope. This simplified the project as a whole, and avoided long delays caused by bureaucratic obstacles. On the other hand, this decision influenced and complicated the optical design of the telescope, as well as the mechanical design of the retractable dome.

3.5 Telescope platform and laboratories

After the removal of the old dome and the 45 cm Gregory-Coudé telescope, the top parts of the building were completely rebuilt (Fig. 6). The flat roof of the building was removed. The old observing room and dome floor (Level 5) were merged to form a large observing laboratory. A new concrete platform for the telescope and for the new dome

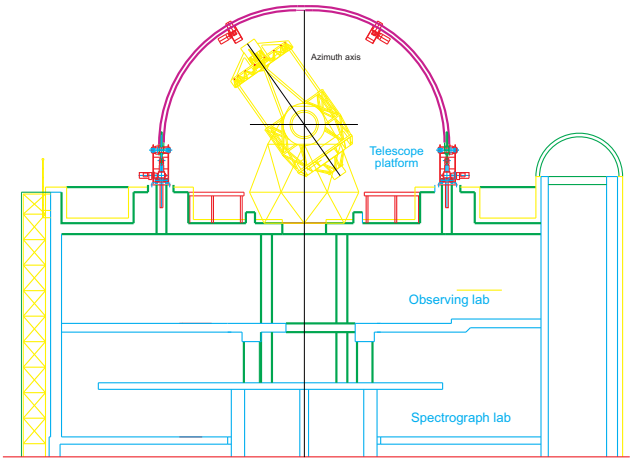

Fig. 6 (online colour at: www.an-journal.org) North-South cut of the top part of the GREGOR building, including the outline of the foldable dome (red colors). Thick green lines indicate the newly built concrete parts, thin blue lines show the pre-existing infrastructure. Thin black lines indicate the azimuth axis, the optical axis of the telescope and the plane of the elevation axis. The telescope structure is indicated in yellow as a generic design.

was built (Level 6). At the same time, the thermal insulation of the roof of the observing laboratory was improved. Concrete columns and steel bars were mounted between the new Level 6 and the two lower levels to increase the stiffness of the telescope platform (see Fig. 6). The spectrograph laboratory in Level 4 was modified by adding a wall to separate the spectrograph optics from the detector area. In Level 3, an existing bedroom was converted into the GREGOR control room for remote operation of the telescope and its instruments. In addition, an outdoor elevator was installed at the south wall of the building, to lift the primary mirror and other heavy equipment to the telescope area.

3.6 Foldable dome

The design of the foldable dome[2] is based on the one used for the 40 cm Dutch Open Telescope (Rutten et al. 1999), but with a diameter of 9 m instead of 7 m. It consists of rotating bows, covered with two layers of a polyester membrane. The inner layer serves as thermal insulation to prevent water condensation on the steel parts. The two main bows are motorized. A Teflon coating on the outside membrane helps to avoid the build-up of an ice layer during periods of snow storms. When closed, the fabric between the steel bars has the shape of a minimum surface. This keeps the dome in shape even during periods of strong wind. Two motorized clamps pull the two halves together to close and seal the dome (see Fig. 7). During observations, the dome is completely open to allow the ambient air to flow across the platform and through the telescope structure. This provides

[2] We use the notion dome, according to the shape (when closed) and the function of the enclosure. The term "tent" is often used, but is somewhat misleading, since a tent is not supposed to fold down when in use.

Fig. 7 (online colour at: www.an-journal.org) Partial view of the nearly closed GREGOR dome. Motorized clamps pull and lock the two halves together, to provide optimum strain to the cloth. *Top*: inside view, *bottom*: outside view.

natural cooling of the telescope and its immediate environment (Sliepen et al. 2010). The dome was designed to survive wind speeds of 70 m/s, when closed, and to be operated at wind speeds up to 20 m/s. It was installed on the GREGOR building already in 2004, and has since then more than once demonstrated that it meets the design requirements. A detailed description of the foldable enclosure for GREGOR is found in Hammerschlag et al. (2012).

3.7 Adaptive optics

Adaptive optics (AO, Berkefeld et al. 2012) is an indispensable part of any large-aperture ground-based solar telescope, in order to reach high spatial resolution anywhere near the diffraction limit. Atmospheric seeing limits the angular resolution for day-time observations to about $1''$, far away from the $0.07''$ diffraction limit of a 1.5 m telescope.The GREGOR optical design includes a standard AO system as well as an option for multi-conjugate adaptive optics (MCAO). Unfortunately, none of the mirrors of the telescope or of the coudé train was suitable for the AO, therefore the deformable mirror (DM) and the tip-tilt mirror (TT) are located on a stationary optical bench in the main observing laboratory (Fig. 9). The additional deformable mirrors needed for the MCAO system will be located on the same bench, and switching from one system the other one is easy.

High-order adaptive optics The GREGOR Adaptive Optics System (GAOS 256) was installed in early 2012. It uses a deformable mirror with 256 actuators and a Shack-Hartmann wavefront sensor with 156 illuminated 10 cm subapertures. The closed-loop bandwidth of the system is 120 Hz, and the maximum number of corrected modes is 170. However, the corrected field of this conventional AO has a radius of only about $5''$. In order to increase the corrected area, the KIS started the development of a multi-conjugated adaptive optics already in 2006 (Schmidt et al. 2010a). The wavefront sensor (WFS) is located as close as possible to the entrance focal plane of the instrument in use, to minimize the light path not seen by the WFS.

Multi-conjugate adaptive optics Conventional adaptive optics corrects mainly the atmospheric distortion near the entrance pupil of the telescope, at or near the optical axis of the telescope. The multi-conjugate adaptive optics system for GREGOR controls the wavefront over a field of view of about one arcminute (see Berkefeld et al. 2010; von der Lühe et al. 2005). To this end, two additional adaptive mirrors are placed in the optical train at locations that correspond to two turbulence layers in the Earth atmosphere at different heights (see Fig. 8). The placement of these mirrors is optimized for observations in the morning, when the seeing is usually better than around noon. During the development of MCAO at KIS, the correction of a larger field of view was successfully demonstrated at the VTT (Berkefeld et al. 2006), and in the meantime, the full system is set up and tested in an optical lab at KIS. Installation of the MCAO system is foreseen for 2013.

3.8 Polarization calibration unit

The GREGOR Polarimetric Unit (GPU) is located in the symmetric beam of the telescope, near the secondary focus, in the light beam between M2 and M3. With the GPU, the instrumental polarization of all surfaces downstream of M2 can be calibrated (Hofmann et al. 2012), therefore, it can be used by all focal plane instruments. Two sets of polarizers and retarders are available for the visible and the near infrared. A polarization model of the GREGOR telescope has been developed, which allows the primary and secondary mirrors to be included in the polarimetric calibration procedure (Balthasar et al. 2011). The GPU was designed with the goal to reach a polarimetric sensitivity of 10^{-4}.

4 Instrumentation

4.1 GRIS

The GRating Infrared Spectrograph (GRIS) builds to a large degree on heritage from the TIP II instrument (Tenerife Infrared Polarimeter, Collados et al. 2007) of the VTT. It uses the same infrared detector, a Rockwell TCM 8600 with

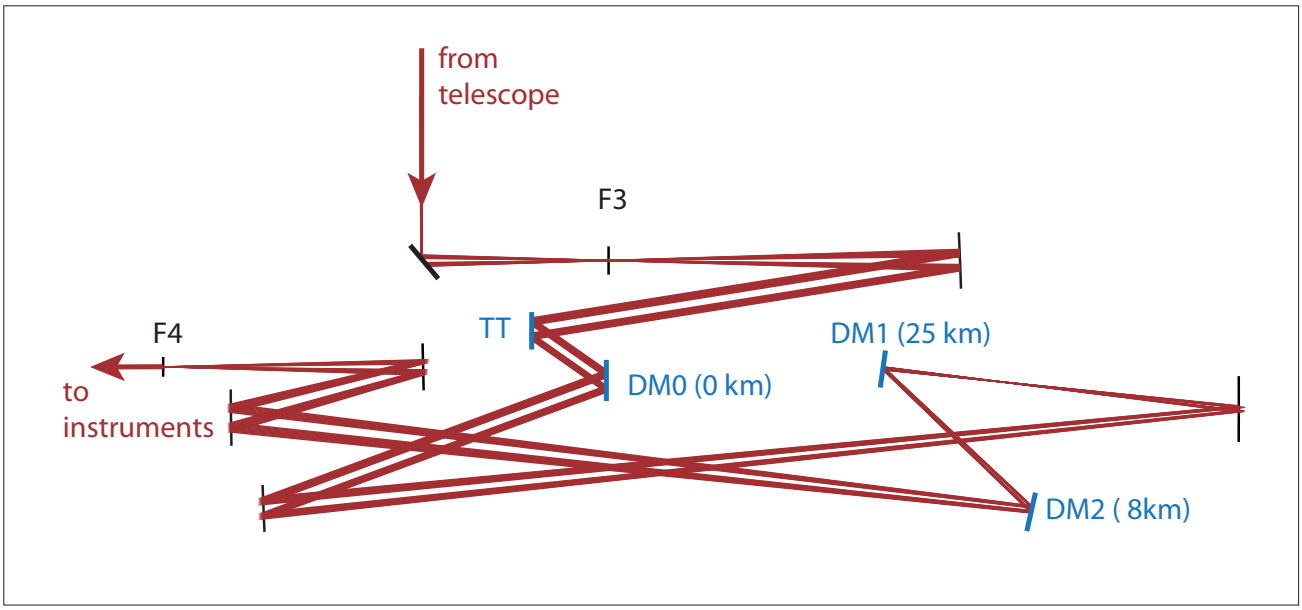

Fig. 8 (online colour at: www.an-journal.org) GREGOR MCAO scheme. DM0 is the ground layer DM, DM1 and DM2 correspond to layers at 8 and 25 km distance, respectively. TT is the tip-tilt mirror, F3 is the coudé focal plane of the telescope. Angles are not to scale.

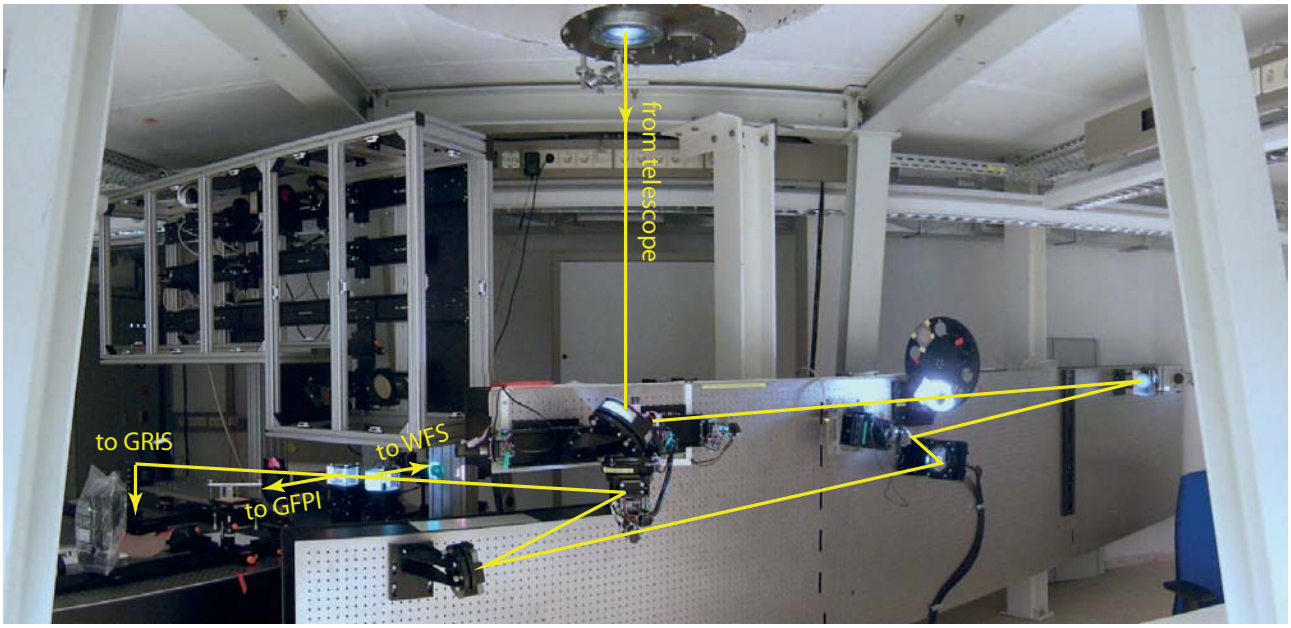

Fig. 9 (online colour at: www.an-journal.org) Wide-angle view of the west side of the GREGOR observing laboratory. The exit window of the telescope is seen in the top center of the image. Some adaptive optics components are mounted on the vertical optical bench. Two beam splitters, one feeding the wavefront sensor, and one to divide the light between GRIS and the GFPI are seen at bottom left. The metal frame of the slit jaw imaging system is located above the beam splitters.

1024×1024 pixels, a square pixel size of 18 μm, and a read-out rate of 30 Hz. The software for data acquisition and data calibration is basically the same as that of TIP II, which is a significant advantage for the users. The image scale is 0.13″/pixel in slit direction, which allows for diffraction-limited critical sampling at a wavelength of 1.5 μm. GRIS includes a horizontal spectrograph that is located one floor beneath the main observing laboratory. The diffraction grating with its 316 grooves per mm, a blaze angle of 63.4 degrees, and linear dimensions of 370 m × 190 mm is re-used from the old spectrograph of the 45 cm Gregory-Coudé telescope, the predecessor of GREGOR in the same building. The spectrograph has a symmetric layout, with two off-axis paraboloids as collimating and imaging mirrors (Fig. 10).

Table 1 Properties and characteristic numbers of the GREGOR telescope and instrumentation.

Description	Value
Telescope:	
Optical design	Gregory
Clear aperture of primary mirror	144 cm
Focal length of primary mirror	2.5 m
Effective focal length of telescope	57.3 m
Field of view (Ø)	150″
Image scale in focus F3	3.6″/mm
Adaptive optics:	
Size of subapertures	10 cm (square)
Illuminated subapertures	156
Actuators of deformable mirror	256
Closed-loop bandwidth	120 Hz
GRIS:	
Wavelength range	1000 to 2200 nm
Slit dimensions (polarimetry)	0.25″×67″
Slit dimensions (spectroscopy)	0.25″×138″
Grating size	370 mm × 190 mm
Grating constant	316 l/mm
Diffraction order for 1560 nm	2 or 3
Spectral pixel size, 3rd order	4 pm
Spectral FOV at 1560 nm, 3rd order	4.0 nm
Spatial pixel size	0.13″
Detector size	1024×1024 pixels
GFPI:	
Wavelength range	530 to 860 nm
Field of view	50″×38″
Pixel size	0.036″
Detector full well	18000 e^-
BBI:	
Field of view	120″×80″
Detector size	4008×2672 pixels
Detector full well	60000 e^-
Wavelength range (detector)	380 nm to 900 nm

The detector is located on the same floor as the spectrograph, but outside the spectrograph room, in order to simplify access to the liquid-nitrogen cooled device. The slit unit, together with the polarization modulator and a slit-jaw camera system is located in the main observing laboratory (Fig. 9). Light passing through the slit is deflected down to the spectrograph through a sealed tube, to avoid air exchange between the two laboratories. GRIS covers a wavelength range between 1000 nm and 2200 nm, which includes the most-used spectral bands at 1083 nm, with the He I triplet and a Si I line, as well as the band at 1565 nm with a Fe I line with a Landé factor of 3. The polarization modulator and analyzer are similar to that of TIP II, with two ferro-electric liquid crystals and a polarizing beam splitter, mounted behind the spectrograph slit. In its polarimetric mode, the slit is 18 mm (67″) high and 70 μm (0.25″) wide. Figures 11 and 12 show intensity spectra obtained during science verification campaigns.

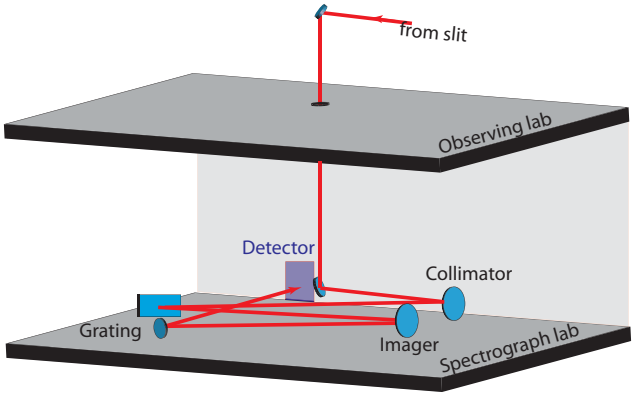

Fig. 10 (online colour at: www.an-journal.org) Schematic drawing of GRIS. Light enters from the entrance slit, located in the observing lab through an opening in the floor to the spectrograph lab. A folding mirror reflects the light to the collimator, which images the entrance pupil to the grating. The imager forms the final image on the detector.

Two-dimensional observations will be enabled in the near future with a slit-scan unit that will be placed directly behind the entrance slit of GRIS. The scan range is intended to be about ±30″, which will allow to cover an area of 67″×60″ in a single scan of 240 steps. The duration of such a scan depends on the desired polarimetric precision.

A slit jaw camera (SJC) system allows recording images of the reflective slit jaws in different wavelength bands. The first channel is equipped with a SolarSpectrum filter for 656.3 nm (Hα), with an FWHM of 50 pm. The second channel records broad-band continuum at wavelengths above 656 nm. The third channel is presently not used. The SJC is equipped with Prosilica CCD cameras. The image scale is 0.078″/pixel, and the field of view is 78″×105″. Figure 9 shows the SJC during setup.

GRIS has been set up under the responsibility of the Instituto de Astrofísica de Canarias (Collados et al. 2008). More information on GRIS can be found in Collados et al. (2012).

4.2 GFPI

The GREGOR Fabry Pérot Interferometer (GFPI) is based on the Göttingen Fabry Pérot Interferometer that was developed by the Universitätssternwarte Göttingen in the early nineties for the VTT. From its predecessor, the GFPI uses the same collimated mount design. In preparation for its move to GREGOR, the instrument underwent a systematic overhaul: In 2005, narrow-band etalons with diameters of 70 mm, and large-format, high-cadence CCD detectors were integrated into the instrument, accompanied by sophisticated computer hard-and software. From 2006 to 2007, the optical design of the GFPI was developed, all necessary optical elements were purchased, and opto-mechanical mounts were manufactured. In addition, in 2007 the instrument was upgraded for Stokes-vector measurements. In 2009, the Leibniz-Institute for Astrophysics in Potsdam took the lead

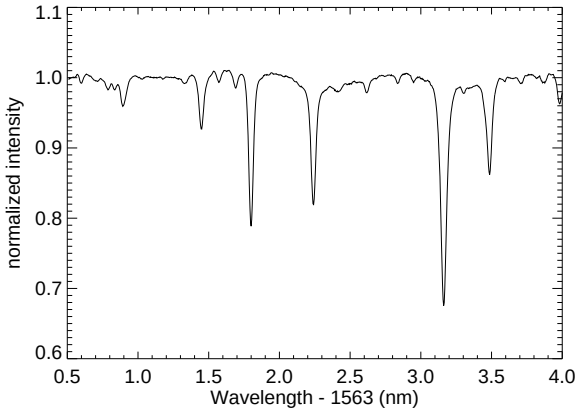

Fig. 11 Spatially averaged spectrum of the 1564 nm region, observed with GRIS. The third diffraction order was used, which leads to a rather large spectral coverage of 4 nm.

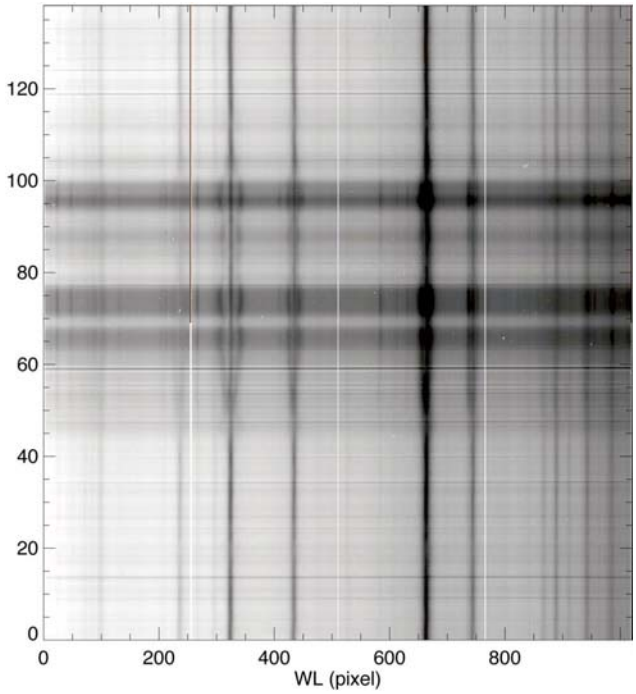

Fig. 12 (online colour at: www.an-journal.org) Single spectrum of a sunspot and its surroundings taken with GRIS in the near infrared at 1.565 μm. The horizontal dark grey bands belong to three umbrae which cause a large Zeeman splitting of some of the spectral lines. The wavelength scale is 40 pm/pixel.

for the further development of the GFPI. At this time, the instrument was dismantled at the VTT and re-installed at GREGOR. During the commissioning phase, the hard- and software was further improved and now also allows for automated observing and calibration procedures (Puschmann et al. 2012b).

Figure 13 shows a scheme of the the light distribution system in the observing lab, and a simplified optical scheme of the GFPI. From the white light entering the observing laboratory, a small fraction is reflected to the wavefront sensor of the AO, then the beam is split by a dichroic beam splitter into visible ($\lambda < 660$ nm) and infrared light. This beam splitter can be replaced by one that splits at 860 nm. The blue-framed box already shows a future upgrade with the Blue Imaging Solar Spectrometer (BLISS, Puschmann et al. 2012b) for the blue part of the visible spectrum ($\lambda < 530$ nm). It is fed with a second dichroic beam splitter. Presently, a broad-band imaging channel for the blue and near UV is located there. The remaining light finally enters the GFPI, shown in the red-framed boxes. A grey beam splitter reflects 5 % of the incoming light to the broad-band channel, while 95 % of the light is transmitted to the narrow-band channel, with its two Etalons and the polarimeter. The spectral resolution of the narrow-band channel is $\Re = \lambda/\triangle\lambda = 250\,000$. The instrument is equipped with two identical CCD detectors with a field of view of $50'' \times 38''$ and an image scale of $0.036''$ per pixel. The data processing software developed for the GFPI includes the possibility for image reconstruction using speckle interferometry (Puschmann & Sailer 2006; Wöger & von der Lühe 2008) or, optionally, deconvolution techniques (Löfdahl 2002). The GFPI can thus obtain diffraction-limited measurements of the intensity and line-of-sight velocity of e.g. a sunspot within a few seconds. A full description of the GFPI can be found in Puschmann et al. (2012c), in Puschmann et al. (2012a) and Puschmann et al. (2012b).

4.3 Broad-band imager

The Broad-Band Imager (BBI, von der Lühe et al. 2012) is designed to take filtergrams at visible wavelengths, down to 390 nm with a field of view of $120'' \times 80''$, and with a pixel scale that allows for diffraction-limited imaging, using post-facto reconstruction techniques. Sequences taken with this instrument will be used to investigate e.g. the fine structure of photospheric granulation (Steiner et al. 2010). The BBI is equipped with a PCO4000 camera with 4008×2672 pixels. A second channel of the BBI is used for Foucault tests to monitor the alignment and optical quality of the telescope. The BBI has been set up by KIS, using mostly existing hardware from the VTT. Figure 14 shows the optical layout of the instrument. The BBI either takes bursts of short-exposure images to allow for post-facto image reconstruction, or it employs a phase-diversity (PD) beam splitter to record simultaneously focused and defocused images for PD reconstruction. Figure 2 is one of the first images taken with the BBI, reconstructed using speckle interferometry.

4.4 Multi-instrument measurements

The arrangement of the focal-plane instruments in the observing laboratory is such that at least two of them can be used simultaneously to observe the same field of view. The light distribution scheme shown in Fig. 13 allows such multi-instrument observations without compromising the photon flux to the respective instrument. Simultaneous observations in different spectral lines, from the near UV, up

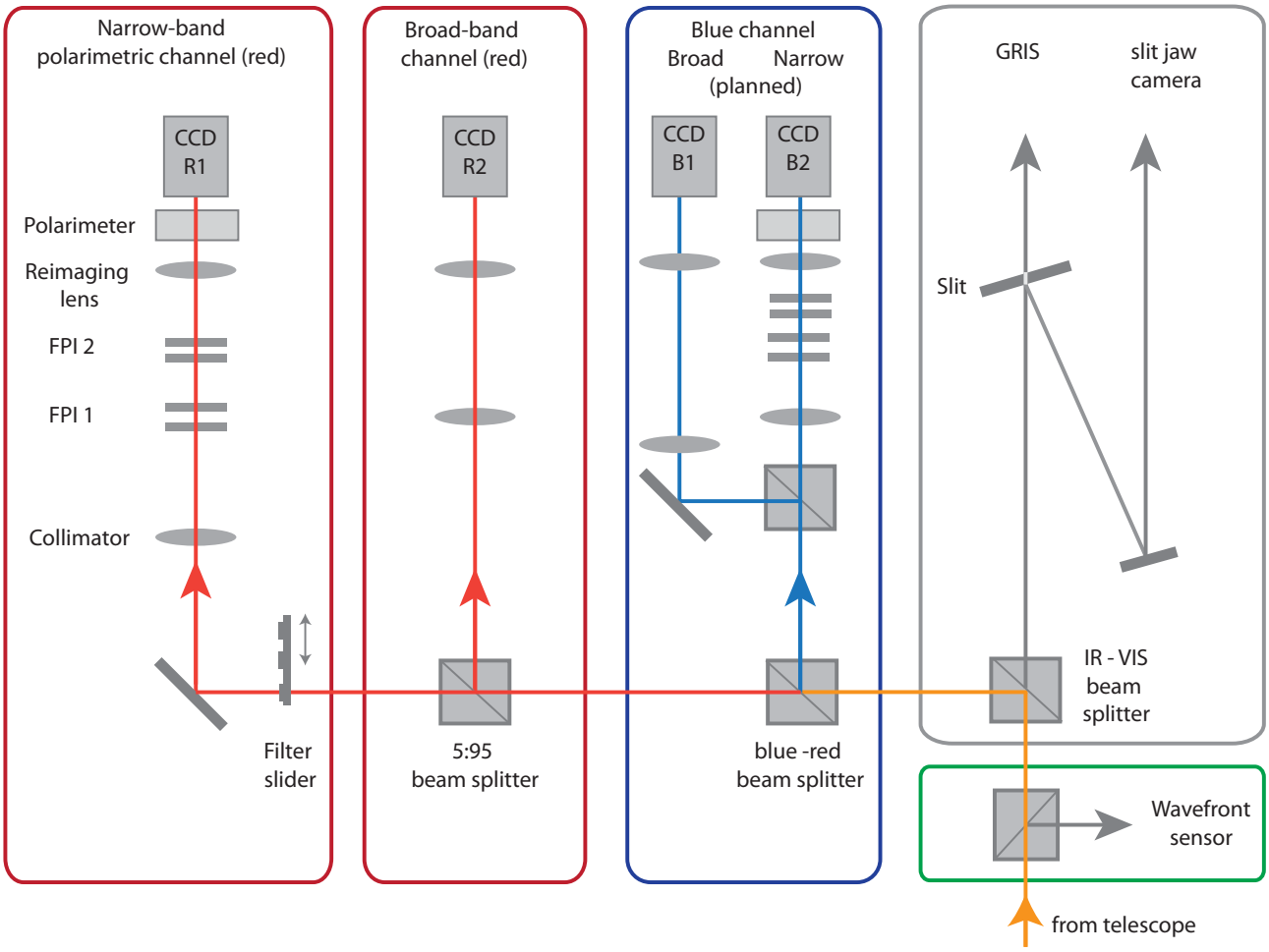

Fig. 13 (online colour at: www.an-journal.org) Scheme of the GREGOR Fabry Pérot Interferometer and the light distribution system. Light from the telescope enters from below. A beam splitter sends a small fraction of the light to the wavefront sensor of the AO. Then, a dichroic beam splitter transmits the infrared light to GRIS and the slit jaw camera, and reflects the visible wavelength band to the GFPI. A blue/red beam splitter deflects the blue part of the light to the blue channel, and the remaining light enters the GFPI, where it is split with a ratio of 5:95 between the broad and the narrow (spectro-polarimetric) channel.

to, say 2.2 μm, provide three-dimensional information of the dynamics and the magnetic field of the photosphere and the lower and mid chromosphere. The combination of GRIS, a grating instrument with a scan unit, and the GFPI, a filter-based spectro-polarimeter will combine the strengths of both systems. The combined measurements will be simultaneous, but not necessarily synchronized, so that each instrument can optimize the integration time according to the photon flux of the observed line and the required signal-to-noise ratio. Similar setups are possible for the Broad-Band Imager (BBI, see Sect. 4.3) and any future instrument that would be located nearby.

5 Second-generation instruments and outlook

5.1 GREGOR@Night

Night-time stellar observations with GREGOR open a new dimension of solar physics. If we study the properties of "solar twins" in the Milky Way, we will better understand the long-term behavior of our Sun, including the relation between magnetic activity and irradiance. To this end, we have to observe a sufficiently large number of stars that are very similar to the Sun, but are in different states of their evolution. The similarity with the Sun includes the spectral type, and the magnetic activity. GREGOR with its 1.5 m aperture is well suited for this purpose, since a large number of nights can be used for this solar twin program. From stellar statistics one estimates the existence of about 5 billions of G2V stars in the Milky Way, or about 3000 such solar twins within a radius of 250 light years around the Sun (Strassmeier et al. 2007).

The instrument foreseen for GREGOR is an Echelle spectrograph based on the SOFIN instrument of the Nordic Optical Telescope, with a spectral resolution up to $\Re = 87\,000$, covering a wavelength range from 350 nm to 1130 nm. For wavelength calibration in the spectral region between 500 nm and 600 nm, an iodine cell can be used. The spectrograph and the telescope will be operated automati-

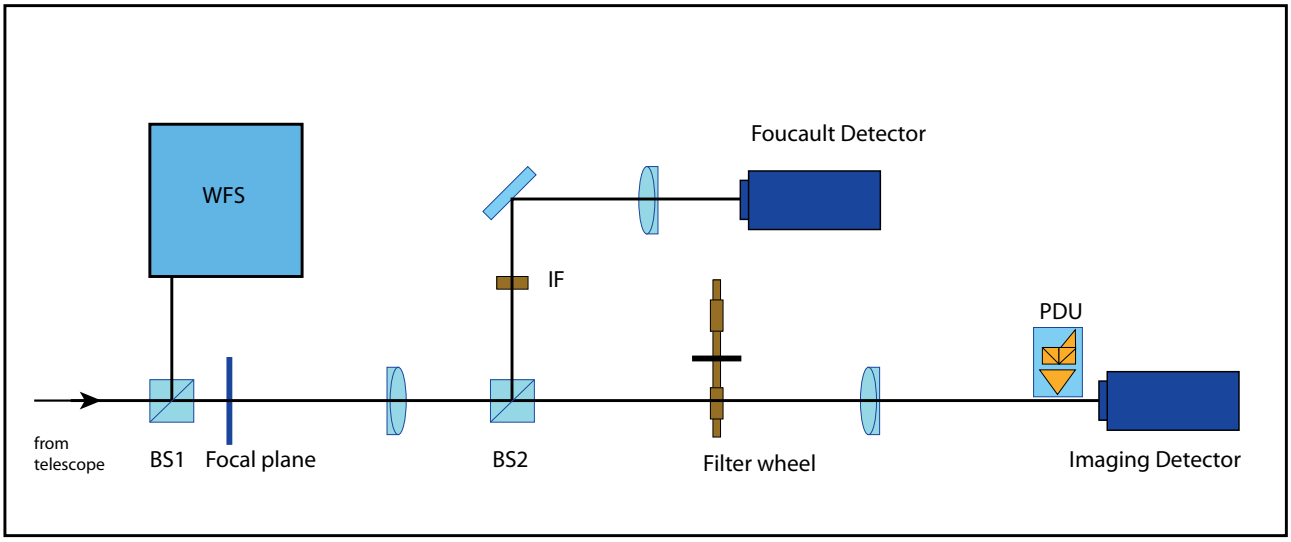

Fig. 14 (online colour at: www.an-journal.org) Layout of the Broad-Band Imager (BBI) of GREGOR. The wavefront sensor of the AO is placed close the entrance focal plane in order to minimize the uncorrected beam. The small device labelled 'PDU' near the imaging detector is a phase diversity beam splitter that can optionally be inserted into the beam.

cally, with a control system based on that of the STELLA telescopes (Strassmeier 2006; Weber et al. 2008), located nearby GREGOR (see Fig. 1). The instrument will be installed next to the GREGOR horizontal spectrograph, and the light feed will be from focus F3 through an existing hole in the floor between the observing and the spectrograph laboratories (Strassmeier et al. 2012).

5.2 ZIMPOL imaging polarimeter

The ZIMPOL III system (Ramelli et al. 2010) will be initially tested at GREGOR for imaging polarimetry with broad-band filters, but the primary goal is to establish new optical configuration which combines a Fabry-Pérot filter with the horizontal spectrograph. A similar setup was tested at IRSOL, Switzerland (Kleint et al. 2011) and appears very promising, as it enables observing at any wavelength without the need of narrow-band pre-filters. It opens also the possibility of obtaining two simultaneous images taken at slightly different wavelengths. This allows, e.g., for simultaneous imaging in the core and a wing of a spectral line or in two opposite line wings.

The ZIMPOL camera has a compact modular design. Backside illuminated CCD sensors with high quantum efficiency and larger number of pixels compared to the previously used CCDs, have been equipped with an optimized masked micro-lens array. Improvements in the stability and the parallelization of the data acquisition processes have increased the efficiency. Successful test measurements have been carried out at IRSOL (Switzerland) and THEMIS (Tenerife). The system is in routine use since 2009, thereby replacing the previous version of the ZIMPOL. Optimization of the ZIMPOL III performance and its adaptation to new applications at the GREGOR telescope are underway.

5.3 GREGOR as a test bed for next generation telescopes

The open design of GREGOR makes this telescope an ideal testbed for the next-generation European Solar Telescope (EST, Collados et al. 2010). That telescope is also designed as an open system (contrary to the Advanced Technology Solar Telescope), and important lessons are to be learnt from GREGOR. The influence of wind on telescope pointing and the thermal behavior of the primary mirror will be studied. One of the critical items of a large on-axis solar telescope is the field stop at the primary image, where a large heat load needs to be efficiently removed. As mentioned earlier, GREGOR produces a heat load of nearly 2000 W concentrated in an area of 2.5 cm in diameter. Efficient removal of this energy by reflection and cooling of the absorbed part are vital. In case of a 4m EST, the power at F1 increases by a factor of seven.

Another issue is the influence of image and spider rotation on the performance of adaptive optics systems. Due to the alt-azimuth mount system, the solar image rotates during the day with variable speed (and sign), and also the image of the telescope pupil rotates, but at a different rate. The latter movement leads to a varying pupil image on the micro-lens array of the WFS. The pupil image includes the spiders that hold the secondary mirror, and these spiders affect the illumination of different subapertures during the day. While this is of little concern for low-order systems, high-order AOs with subapertures of 10 cm or less, need to take this effect into account.

The foldable dome is also a prototype in view of much larger units that would be needed, e.g., for the EST. The GREGOR dome is therefore equipped with laser sensors to measure mechanical deformations, and with pressure sensors to study elastic deformations of the dome as a function

of wind speed and direction (Sliepen et al. 2010). It should be mentioned that the open GREGOR telescope, together with its retractable dome, will inevitably lead to dust deposition on the primary mirror.

5.4 Next steps

The ongoing science verification phase will reveal strengths and weaknesses of the new telescope, which in turn will lead to improvements. This is a continuous process that will not end when GREGOR becomes available for regular scientific observations in the near future.

Acknowledgements. The 1.5 m GREGOR solar telescope was build by a German consortium under the leadership of the Kiepenheuer-Institut für Sonnenphysik in Freiburg with the Leibniz-Institut für Astrophysik Potsdam, the Institut für Astrophysik Göttingen, and the Max-Planck-Institut für Sonnensystemforschung in Katlenburg-Lindau as partners, and with contributions by the Instituto de Astrofísica de Canarias and the Astronomical Institute of the Academy of Sciences of the Czech Republic.

References

Ball, W.T., Unruh, Y.C., Krivova, N.A., Solanki, S., Harder, J.W.: 2011, A&A 530, A71
Ball, W.T., Unruh, Y.C., Krivova, N.A., Solanki, S., Wenzler, T., Mortlock, D.J., Jaffe, A.H.: 2012, A&A 541, A27
Balthasar, H., Bello González, N., Collados, et al.: 2011, in: J.R. Kuhn, S. V. Berdyugina, D.M. Harrington, S.L. Keil, H. Lin, T. Rimmele, J. Trujillo-Bueno (eds.), *Solar Polarization Workshop 6*, ASPC 437, p. 351
Barthol, P., Gandorfer, A., Solanki, S.K., et al.: 2011, Sol. Phys. 268, 1
Bello González, N., Franz, M., Martínez Pillet, V., Bonet, J.A., Solanki, S.K., del Toro Iniesta, J.C., Schmidt, W., et al.: 2010, ApJ 723, L134
Berkefeld, T., Soltau, D., von der Lühe, O.: 2006, in: B.L. Ellerbroek, D. Bonaccini Calia (eds.), *Advances in Adaptive Optics II*, SPIE 6272, p. 627205
Berkefeld, T., Soltau, D., Schmidt, D., von der Lühe, O.: 2010, Appl.Optics 49, G155
Berkefeld, Th., Schmidt, D., Soltau, D., von der Lühe, O., Heidecke, F.: 2012, AN 333, 863
Bharti, L., Joshi, C., Jaaffrey, S.N.A., Jain, R.: 2009, MNRAS 393, 65
Cao, W., Gorceix, N., Coulter, R., Coulter, A., Goode, P.R.: 2010, in: L.M. Stepp, R. Gilmozzi, H.J. Hall (eds.), *Ground-Based and Airborne Instrumentation for Astronomy III*, SPIE 7733, p. 773330
Carlsson, M.: 2007, in: P. Heinzel, I. Dorotovič, R.J. Rutten (eds.), *The Physics of Chromospheric Plasmas*, ASPC 368, p. 49
Collados, M., Lagg, A., Díaz Garcí A, J.J., Hernández Suárez, E., López López, R., Páez Mañá, E., Solanki, S.K.: 2007, in: P. Heinzel, I. Dorotovič, R.J. Rutten (eds.), *The Physics of Chromospheric Plasmas*, ASPC 368, p. 611
Collados, M., Calcines, A., Díaz, J.J., Hernández, E., López, R., Páez, E.: 2008, in: I.S. McLean, M.M. Casali (eds.), *Ground-Based and Airborne Instrumentation for Astronomy II*, SPIE 7014, p. 70145Z
Collados, M., Bettonvil, F., Cavaller, L., et al.: 2010, AN 331, 615
Collados, M., López, R., Páez, E., et al.: 2012, AN 333, 872
Denker, C., von der Lühe, O., Feller, A., et al.: 2012, AN 333, 810
de Wijn, A.G., Stenflo, J.O., Solanki, S.K., Tsuneta, S.: 2009, Space Sci.Rev. 144, 275
Engvold, O., Andersen, T.: 1990, LEST Foundation Design Report
Franz, M., Schlichenmaier, R.: 2009, A&A 508, 1453
Fröhlich, C.: 2006, Space Sci.Rev. 125, 53
Fügner, D., Granzer, T., Strassmeier, K.G.: 2011, in: C. Johns-Krull, M.K. Browning, A.A. West (eds.), *Cool Stars, Stellar Systems, and the Sun*, ASPC 448, p. 863
Granzer, T., Halbgewachs, C., Volkmer, R., Soltau, D.: 2012, AN 333, 823
Grossmann-Doerth, U., Schüssler, M., Steiner, O.: 1998, A&A 337, 928
Halbgewachs, C., Caligari, P., Glogowski, K., et al.: 2012, AN 333, 840
Hammerschlag, R.H., Kommers, J.N., Visser, S., et al.: 2012, AN 333, 830
Harder, J., Fontenla, J., White, O., Rottman, G., Woods, T.: 2005, Mem. Soc. Astron. Ital. 76, 735
Hasan, S.S., van Ballegooijen, A.A., Kalkofen, W., Steiner, O.: 2005, ApJ 631, 1270
Harvey, J.W.: 2009, in: S.V. Berdyugina, K.N. Nagendra, R. Ramelli (eds.), *Solar Polarization 5: In Honor of Jan Stenflo*, ASPC 405, p. 157
Hofmann, A., Arlt, K., Balthasar, H., et al.: 2012, AN 333, 854
Joshi, J., Pietarila, A., Hirzberger, J., Solanki, S.K., Aznar Cuadrado, R., Merenda, L.: 2011, ApJ 740, L55
Judge, P., Knölker, M., Schmidt, W., Steiner, O.: 2010, ApJ 720, 776
Keil, S.L., Rimmele, T.R., Wagner, J., ATST team: 2010, AN 331, 609
Kleint, L., Feller, A., Gisler, D.: 2011, A&A 529, A78
Kneer, F.: 2012, AN 333, 790
Kosugi, T., Matsuzaki, K., Sakao, T., et al.: 2007, Sol. Phys. 243, 3
Krivova, N.A., Solanki, S.K., Fligge, M., Unruh, Y.C.: 2003, A&A 399, L1
Krivova, N.A., Solanki, S.K., Floyd, L.: 2006, A&A 452, 631
Lagg, A., Solanki, S.K., Riethmüller, T.L., et al.: 2010, ApJ 723, L164
Löfdahl, M.G.: 2002, in: P.J. Bones, M.A. Fiddy, R.P. Millane (eds.), *Image Reconstruction from Incomplete Data*, SPIE 4792, p. 146
Penn, M.J., Livingston, W.: 2011, in: D. Choudhary, K.G. Strassmeier (eds.), *The Physics of Sun and Star Spots*, IAU Symp. 273, p. 126
Puschmann, K.G., Sailer, M.: 2006, A&A 454, 1011
Puschmann, K.G., Balthasar, H., Bauer, S.-M., et al.: 2012a, ASPC 463, astro-ph/1111.5509
Puschmann, K.G., Balthasar, H., Bello Gonzalez, N., et al.: 2012b, astro-ph/1207.2084
Puschmann, K.G., Denker, C., Kneer, F., et al.: 2012c, AN 333, 880
Ramelli, R., Balemi, S., Bianda, M., et al.: 2010, in: I.S. McLean, S.K. Ramsay, H. Takami (eds.), *Ground-based and Airborne Instrumentation for Astronomy III*, SPIE 7735, p. 77351Y
Rezaei, R., Beck, C., Schmidt, W.: 2012a, A&A 541, A60
Rezaei, R., Bello González, N., Schlichenmaier, R.: 2012b, A&A 537, A19
Riethmüller, T.L., Solanki, S.K., Lagg, A.: 2008, ApJ 678, L157

Riethmüller, T.L., Solanki, S.K., Martínez Pillet, V.: 2010, ApJ 723, L169
Rutten, R.J.: 2010, Mem. Soc. Astron. Ital. 81, 565
Scharmer, G.B., Gudiksen, B.V., Kiselman, D., Löfdahl, M.G., Rouppe van der Voort, L.H.M.: 2002, Nature 420, 151
Scharmer, G.B., Henriques, V.M.J., Kiselman, D., de la Cruz Rodríguez, J.: 2011, Sci 333, 316
Scharmer, G.B., Kiselman, D., Löfdahl, M.G., Rouppe van der Voort, L.H.M.: 2003, in: J. Trujillo-Bueno, J. Sanchez Almeida (eds.), *Solar Polarization*, ASPC 307, p. 3
Scherrer, P.H., Bogart, R.S., Bush, R.I., et al.: 1995, Sol. Phys. 162, 129
Scherrer, P.H., Schou, J., Bush, R.I., et al.: 2012, Sol. Phys. 275, 207
Schmidt, D., Berkefeld, T., Feger, B., Heidecke, F.: 2010a, in: B.L. Ellerbroek, M. Hart, N. Hubin, P.L. Wizinowich (eds.), *Adaptive Optics Systems II*, SPIE 7736, p. 773607
Schmidt, W., Solanki, S.K., Barthol, P., et al.: 2010b, AN 331, 601
Schmidt, W., von der Lühe, O., Volkmer, R., et al.: 2012, astro-ph/1202.4289
Schüssler, M., Vögler, A.: 2006, ApJ 641, L73
Sliepen, G., Jägers, A.P.L., Hammerschlag, R.H., Bettonvil, F.C.M.: 2010, in: L.M. Stepp, R. Gilmozzi, H.J. Hall (eds.), *Ground-Based and Airborne Telescopes III*, SPIE 7733, p. 773332
Solanki, S.K., Barthol, P., Danilovic, S., et al.: 2010, ApJ 723, L127
Soltau, D., Volkmer, R., von der Lühe, O., Berkefeld, Th.: 2012, AN 333, 847
Spruit, H.C., Scharmer, G.B.: 2006, A&A 447, 343
Steiner, O., Franz, M., Bello González, N., et al.: 2010, ApJ 723, L180
Strassmeier, K.G.: 2006, Ap&SS 304, 397
Strassmeier, K.G., Woche, M., Granzer, T., Andersen, M.I., Schmidt, W., Koubsky, P.: 2007, in: F. Kneer, K.G. Puschmann, A.D. Wittmann (eds.), *Modern Solar Facilities – Advanced Solar Science*, p. 51
Strassmeier, K.G., Ilyin, I.V., Woche, M., et al.: 2012, AN 333, 901
Volkmer, R., von der Lühe, O., Kneer, F., et al.: 2006, in: L.M. Stepp (ed.), *Ground-Based and Airborne Telescopes*, SPIE 6267, p. 62670W
Volkmer, R., Eisenträger, P., Emde, P., et al.: 2012, AN 333, 816
von der Lühe, O., Schmidt, W., Soltau, D., Kneer, F., Staude, J.: 2000, in: A. Wilson (ed.), *The Solar Cycle and Terrestrial Climate, Solar and Space weather*, ESA-SP 463, p. 629
von der Lühe, O., Berkefeld, T., Soltau, D.: 2005, Comptes Rendus Physique 6, 1139
von der Lühe, O., Volkmer, R., Kentischer, T.J., Geißler, R.: 2012, AN 333, 894
Weber, M., Granzer, T., Strassmeier, K.G., Woche, M.: 2008, in: A. Bridger, N.M. Radziwill (eds.), *Advanced Software and Control for Astronomy II*, SPIE 7019, p. 70190L
Wedemeyer-Böhm, S., Lagg, A., Nordlund, Å.: 2009, Space Sci.Rev. 144, 317
Wedemeyer-Böhm, S., Scullion, E., Steiner, O., Rouppe van der Voort, L., de La Cruz Rodriguez, J., Fedun, V., Erdélyi, R.: 2012, Nature 486, 505
Wenzler, T., Solanki, S.K., Krivova, N.A., Fröhlich, C.: 2006, A&A 460, 583
Wöger, F., von der Lühe, O.: 2008, in: in: A. Bridger, N.M. Radziwill (eds.), *Advanced Software and Control for Astronomy II*, SPIE 7019, p. 70191E
Woods, T.N., Rottman, G.: 2005, Sol. Phys. 230, 375